

---

# LATENT WATERMARK: INJECT AND DETECT WATERMARKS IN LATENT DIFFUSION SPACE

---

**Zheling Meng**

Center for Research on  
Intelligent Perception and Computing,  
State Key Laboratory of  
Multimodal Artificial Intelligence Systems,  
Institute of Automation,  
Chinese Academy of Sciences  
zheling.meng@cripac.ia.ac.cn

**Bo Peng**

Center for Research on  
Intelligent Perception and Computing,  
State Key Laboratory of  
Multimodal Artificial Intelligence Systems,  
Institute of Automation,  
Chinese Academy of Sciences  
bo.peng@nlpr.ia.ac.cn

**Jing Dong\***

Center for Research on  
Intelligent Perception and Computing,  
State Key Laboratory of  
Multimodal Artificial Intelligence Systems,  
Institute of Automation,  
Chinese Academy of Sciences  
jdong@nlpr.ia.ac.cn

## ABSTRACT

Watermarking is a tool for actively identifying and attributing the images generated by latent diffusion models. Existing methods face the dilemma of watermark robustness and image quality. The reason for this dilemma is that watermark detection is performed in pixel space, implying an intrinsic link between image quality and watermark robustness. In this paper, we highlight that an effective solution to the problem is to both inject and detect watermarks in latent space, and propose Latent Watermark (LW) with a progressive training strategy. Experiments show that compared to the recently proposed methods such as StegaStamp, StableSignature, RoSteALS and TreeRing, LW not only surpasses them in terms of robustness but also offers superior image quality. When we inject 64-bit messages, LW can achieve an identification performance close to 100% and an attribution performance above 97% under 9 single-attack scenarios and one all-attack scenario. Our code will be available on GitHub.

**Keywords** Latent diffusion model, Watermark, Latent space

## 1 Introduction

Recently, latent diffusion models Nichol et al. [2022], Rombach et al. [2022], Gu et al. [2022] are developing rapidly and have made many important breakthroughs in high-fidelity and controllable image generation. Trained on a large scale dataset, a latent diffusion model can generate images with high resolution and quality according to text descriptions Rombach et al. [2022]. By efficient and effective fine-tuning Hu et al. [2021], Ruiz et al. [2023], Xie et al. [2023], some methods can generate images on specific scenarios and subjects. Besides open-source models Hug, many online platforms also provide similar services to the public mid [2022], wuk [2022]. While bringing convenience to our daily lives and works, they inevitably bring information security risks to our society. For example, some individuals use diffusion models to fabricate fake news, creating social panic and disrupting social order Barrett et al. [2023]. And some people create and spread rumors to defame the reputation of others. Methods that can identify images generated by latent diffusion models and determine their sources are urgently needed.

---

\*Corresponding Author

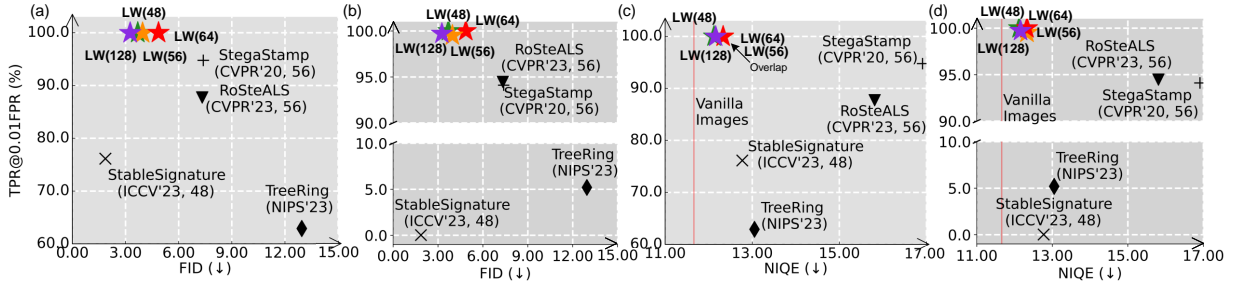


Figure 1: The scatter-plots of the trade-off between image quality and watermark robustness on MS-COCO 2017 captions Lin et al. [2014] for StegaStamp Tancik et al. [2020], StableSignature Fernandez et al. [2023], RoSteALS Bui et al. [2023], TreeRing Wen et al. [2023], as well as our proposed Latent Watermark (LW). (a) FID (↓) versus average TPR@0.01FPR (↑) under the 9 single-attack scenarios. (b) FID (↓) versus TPR@0.01FPR (↑) under the all-attack scenario. (c) NIQE (↓) versus average TPR@0.01FPR (↑) under the 9 single-attack scenarios. (d) NIQE (↓) versus TPR@0.01FPR (↑) under the all-attack scenario.

There are two main routes for identifying generated images, i.e. passive identification and active identification Raja [2021]. Passive identification methods learn and extract forgery traces left by generators in spatial or frequency domain Wang et al. [2020], Qian et al. [2020], Sun et al. [2022], Wang et al. [2023a], Chai et al. [2020]. However, they usually cannot accurately identify generators unseen in training sets Corvi et al. [2023], Lorenz et al. [2023], Ricker et al. [2023]. Besides, they cannot attribute users who access the services to generate images. In contrast, active identification injects an invisible watermark into generated images before releasing them Fernandez et al. [2022], Tancik et al. [2020], Xiong et al. [2023], Nguyen et al. [2023], Bui et al. [2023], Fernandez et al. [2023], Zhao et al. [2023a]. The watermarks, usually in the form of multi-bit messages, can help to identify generated images (identification task) and attribute their sources (attribution task). The watermarking methods for latent diffusion models are attracting more and more attention.

Existing watermarking methods for latent diffusion models can be classified into three categories, i.e. executing watermark algorithms before Fernandez et al. [2023], Zhao et al. [2023a], during Xiong et al. [2023], Nguyen et al. [2023], Wen et al. [2023], and after generating images Fernandez et al. [2022], Tancik et al. [2020], Bui et al. [2023]. A good watermarking method should satisfy strong robustness and high image quality. Strong robustness helps resist attacks from intentional and unintentional damages. High image quality can alleviate the concerns among model developers regarding its potential negative impact on their generative models, thereby encouraging the widespread application of the method. The injection of watermarks should be done in an imperceptible manner and should not change or even limit the generation ability of vanilla models. However, existing methods often exhibit a trade-off between image quality and watermark robustness. We evaluate four recently proposed methods that have been reported to have good performance, i.e. SteagStamp Tancik et al. [2020], StableSignature Fernandez et al. [2023], RoSteALS Bui et al. [2023] and TreeRing Wen et al. [2023]. The robustness is evaluated under 9 single-attack scenarios and one all-attack scenario. And we plot the results in Fig.1. It can be seen that SteagStamp and RoSteALS show better robustness (better TPR@0.01FPR) with a cost of image quality (worse FID and NIQE) while StableSignature shows a better image quality (better FID and NIQE) with a lower TPR@0.01FPR under the attacks. For TreeRing, it significantly changes the distribution of generated images (worse FID) and fails to achieve satisfactory robustness. And its detection method is difficult to attribute users, limiting its utility in certain scenarios.

We highlight that the reason for this dilemma is that the methods Fernandez et al. [2022], Tancik et al. [2020], Xiong et al. [2023], Nguyen et al. [2023], Bui et al. [2023], Fernandez et al. [2023], Zhao et al. [2023a] all decode watermarks in pixel space. It guides models to inject watermarks in a low-level manner of pixel perturbation. When the magnitude of this perturbation is small, it is not enough to resist various attacks. When the magnitude is large, image quality is severely affected. Although TreeRing Wen et al. [2023] does not rely on this manner, it places higher requirements on the precise forward and backward diffusion processes, which in turn increases the difficulty of watermark robustness. If both injecting and detecting are moved to latent space, models can learn to generate a high-level perturbation. It weakens the link between image quality and watermark robustness with latent encoders and decoders. The experiments show that it alleviates the trade-off significantly, as shown in Fig.1, especially compared with the method RoSteALS which injects watermarks in latent space but detects them in pixel space Bui et al. [2023].

Specifically, we propose **Latent Watermark (LW)** to watermark and detect images generated by latent diffusion models in latent space. Compared with previous methods, the fundamental difference is that not only the injection but also the

detection of watermarks is performed in latent space. However, according to our experiments, injecting and detecting watermarks using LW with a high image quality and robustness is not easy. We find that the way to train the model will seriously affect its performance. In our work, a three-step progressive training strategy is proposed to train the watermark-related modules from local to global while freezing the weights of the vanilla model. The experiments on MS-COCO 2017 Lin et al. [2014] and Flickr30k Young et al. [2014] captions show that our method has **stronger robustness** and **higher image quality** at the same time as shown in Fig.1 and Fig.1. We also study the effectiveness of each training step, the position for watermark injection and the size of training data on the performance of LW. And additional necessary discussions are also conducted.

## 2 Related Work

### 2.1 Latent Diffusion Model

Diffusion probabilistic models Sohl-Dickstein et al. [2015], Ho et al. [2020] are proposed to learn a data distribution  $p(\tilde{x})$  from a real distribution  $q(x)$  by the Markov forward and backward diffusion process. Specifically, they train a noise predictor  $\epsilon_\theta(\tilde{x}_t, t)$  to generate an image  $\tilde{x}_0$  from a sampled Gaussian noise  $\tilde{x}_T$  by estimating the noises and performing denoising for  $T$  steps. In order to speed up the generation process, Song et al. propose Denoising Diffusion Implicit Model (DDIM) Song et al. [2020] to reduce the standard 1000-step denoising process to fewer, usually 50 steps. To reduce computational resource requirements while retaining the quality, Latent Diffusion Model (LDM) Rombach et al. [2022] performs the diffusion process in a latent space and becomes a standard paradigm for image generation using diffusion models Nichol et al. [2022], Rombach et al. [2022], Gu et al. [2022]. LDM performs denoising in the latent space with lower resolution and then uses a latent decoder  $Dec(\cdot)$  to generate human-understandable images with higher resolution:

$$\begin{aligned}\tilde{x} &= Dec(\tilde{z}_0) \\ \tilde{z}_{t-1} &= \frac{1}{\sqrt{\alpha_t}} \left( \tilde{z}_t - \frac{1 - \alpha_t}{\sqrt{1 - \bar{\alpha}_t}} \epsilon_\theta(\tilde{z}_t, t) \right) \quad (t = 1, 2, \dots, T)\end{aligned}\tag{1}$$

where  $\alpha_t = 1 - \beta_t$ ,  $\bar{\alpha}_t = \prod_{i=1}^t \alpha_i$  and  $\beta \in (0, 1)$  is a scheduled noise variance. For training the noise predictor  $\epsilon_\theta(\tilde{z}_t, t)$  in the latent space, LDM also includes a latent encoder  $Enc(\cdot)$  to encode training images. In this paper, Stable Diffusion (SD) Rombach et al. [2022], a classic model implementation for LDM, is used to introduce and evaluate our watermarking method. The shape of  $\tilde{z}_t$  and  $\tilde{x}$  is (4, 64, 64) and (3, 512, 512) respectively.

### 2.2 Watermarks for Latent Diffusion Models

Watermarking methods typically inject information as a series of bits within generated images in a subtly or imperceptibly manner. It allows for the determination of whether an image is generated and by which user through the detection of this injected information. For latent diffusion models, the methods can be classified into three categories according to the order of watermark algorithm execution and image generation.

Execute watermark algorithms before generation. The methods allow diffusion models to directly generate watermarked images without introducing any other modules. Zhao et al. [2023a] train unconditional or class-conditional models using watermarked training images, and generate watermarked images using a trigger prompt for text-conditional models. StableSignature Fernandez et al. [2023] roots a watermark into model weights by training a message encoder-decoder and fine-tuning the diffusion model. Once training is completed, both methods cannot change the injected messages.

Execute watermark algorithms during generation. Stable Messenger Nguyen et al. [2023] embeds an encoded bit message into latent diffusion space and decodes it from generated images. The work Xiong et al. [2023] carefully designs the fusion method for encoded messages and latent images. It also proposes a secure mechanism that can overcome watermark injection escape caused by simply commenting out the codes. As the most fundamental difference from our method, they both detect watermarks in pixel space via training another decoder. TreeRing Wen et al. [2023] directly writes messages in the spectrum of sampled noises and detects the messages by Gaussian noising and spectral transformation. However, it fails to attribute users, limiting its application scenarios. The proposed LW belongs to this category.

Execute watermark algorithms post generation. Given a generated image, the methods generate a generator-independent watermark and inject it into the image. StegaStamp Tancik et al. [2020] follows this way and adopts many augmentation methods in the training stage to enhance its robustness. Inspired by self-supervised learning, Fernandez et al. [2022] propose SSL-Watermarking to optimize an invisible watermark image-by-image and detect it by estimating

vector cosine angles. RoSteALS Bui et al. [2023] encodes input images into a latent space by a well trained autoencoder and then injects encoded messages. Same as Nguyen et al. [2023] and Xiong et al. [2023], the methods also detect watermarks in pixel space via training another decoder.

### 2.3 Watermark Attacks

The purpose of watermark attack experiments is to evaluate the robustness of watermarking methods when faced with malicious or unintentional image corruptions in practice. The common attacks can be classified into three categories, i.e. destructive attacks, constructive attacks and reconstructive attacks Zhao et al. [2023b]. Destructive attacks include brightness distortion, contrast distortion, JPEG compression and Gaussian noising. Constructive attacks mainly include some denoising algorithms using Gaussian kernels or Block-Matching and 3D filtering (BM3D) Dabov et al. [2007]. Recently, Zhao et al. propose reconstructive attacks Zhao et al. [2023b] to erase watermarks. They use an image reconstruction model, such as a diffusion model or a variational autoencoder, to encode semantic features of an image and regenerate it. The work highlights that a simple reconstruction model can erase watermarks injected by most existing methods.

## 3 Methods

### 3.1 Threat Model

There are three agents involved in our threat model, i.e. a service provider, a user and a regulator. Owning a latent diffusion model, the service provider provides image generation services to the public through an API. The generated images are watermarked before being released. Given a text description, the user calls the diffusion model through the API to obtain generated images. The regulator, from the service provider or government departments, completes the following two tasks by detecting watermarks:

- Identification: Determine whether an image is generated by the service provider.
- Attribution: Determine which user generates the image through the API.

The difference between the two is that the latter requires an exact match of bits. Due to unintentional and intentional damages, there are differences in image quality between generated and detected images but the contents of detected images can still be accurately understood by humans. We formally summarize the threat model as follows. We denote  $\tilde{x}$  as a generated image, distinguished from a real image  $x$ .

- Service Provider: She owns a latent diffusion model  $\epsilon_\theta$  and provides an API to the public to generate images watermarked by an algorithm  $\mathcal{T}$ .  $\mathcal{T}$  injects identity information in bit form into generated images while maintaining image quality so that it cannot be perceived by users.
- User: She obtains an image  $\tilde{x}$  conditioned on a text description  $c$  through the API.  $\tilde{x}$  can be changed into  $\tilde{x}'$  by common attacks as mentioned in Sec.2.3. And humans have a consistent understanding of  $\tilde{x}$  and  $\tilde{x}'$ .
- Regulator: Given  $\mathcal{T}$ , the regulator tries to identify and attribute  $\tilde{x}'$ .

### 3.2 Latent Watermark

Fig.2 (a) shows the structure of LW. LW is composed of a message encoder  $Enc_M(\cdot)$ , a message coupler  $C(\cdot, \cdot)$ , a message decoupler  $DC(\cdot)$  and a message decoder  $Dec_M(\cdot)$ . Besides, a latent diffusion model, including a latent encoder  $Enc(\cdot)$ , a noise predictor  $\epsilon_\theta(\tilde{z}_t, t)$  and a latent decoder  $Dec(\cdot)$ , is also needed.

In the stage of injecting watermarks, given a  $n$ -bit message,  $Enc_M(\cdot)$  first encodes it into the latent space. Then,  $C(\cdot, \cdot)$  fuses the latent image  $\tilde{z}$  from  $\epsilon_\theta(\tilde{z}_t, t)$  with the encoded message to obtain  $\tilde{z}'$ . Next,  $\tilde{z}'$  is decoded by  $Dec(\cdot)$  to generate an image  $\tilde{x}$ . The injecting process can be expressed as Eq.2:

$$\tilde{x} = Dec(C(\tilde{z}, Enc_M(M))) \quad (2)$$

where  $M \in \{0, 1\}^n$  is a  $n$ -bit message. In the experiments, we find that choosing different channels to fuse messages will bring different performance. According to the results in Tab.3, we design  $C(\cdot, \cdot)$  to fuse the first channel of  $\tilde{z}$  with the encoded messages, as shown in Fig.2 (a) and Eq.3:

$$\begin{aligned} \tilde{z}' &= C(\tilde{z}, Enc_M(M)) \\ &= C(\tilde{z}_{(0)}, Enc_M(M)) \oplus \tilde{z}_{(1)} \oplus \tilde{z}_{(2)} \oplus \tilde{z}_{(3)} \end{aligned} \quad (3)$$

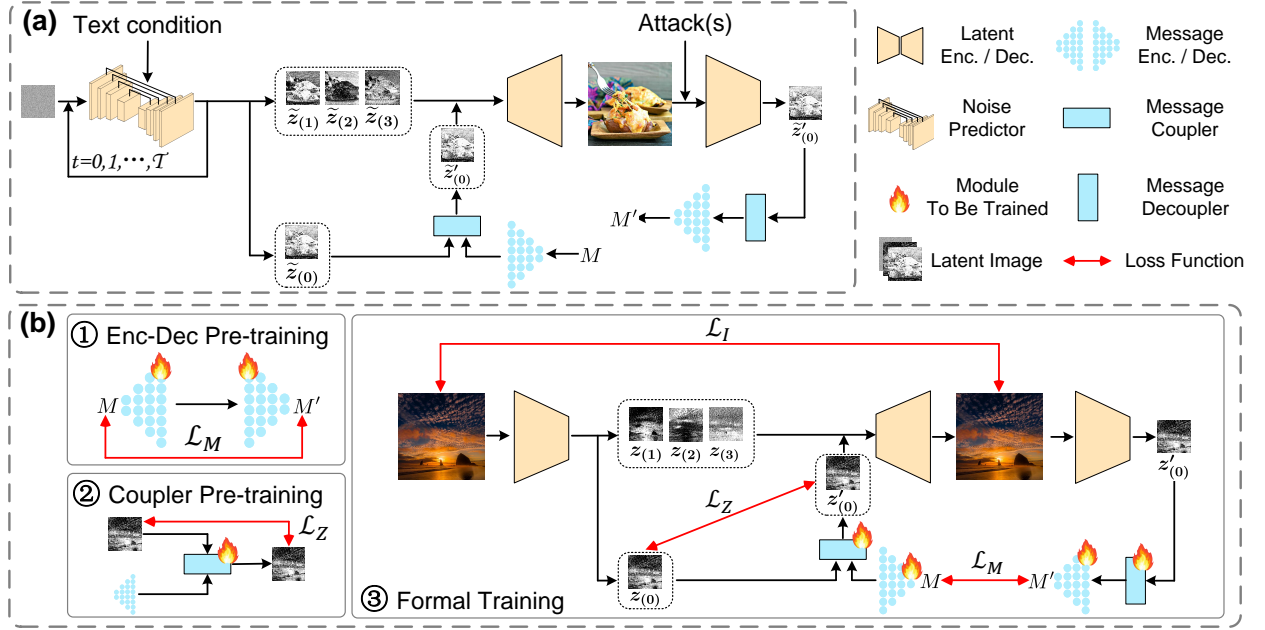


Figure 2: The proposed methods. (a) The structure of LW. (b) The three-step progressive training strategy.  $M$ :  $n$ -bit messages.  $z_{(l)}$ :  $l$ -th channel of latent image  $z$ .

where  $\oplus$  is concatenation along the channel dimension and  $\tilde{z}_{(l)}$  is  $l$ -th channel of  $\tilde{z}$  ( $l = \{0, 1, 2, 3\}$ ).  $Enc_M(M)$  has the same shape with  $\tilde{z}_{(l)}$ .

In the stage of detecting watermarks,  $Enc(\cdot)$  is used to encode an image  $\tilde{x}'$  into the latent space. Then  $DC(\cdot)$  decouples the encoded message from the first channel of the latent image. Finally,  $Dec_M(\cdot)$  outputs the decoding result in bit form. The detecting process can be expressed as Eq.4:

$$\begin{aligned} M' &= Dec_M(DC(\tilde{z}'_{(0)})) \\ \tilde{z}' &= Enc(\tilde{x}') \end{aligned} \quad (4)$$

where  $M' \in \{0, 1\}^n$  is the decoded message.

### 3.3 Three-Step Progressive Training Strategy

As pointed out in Sec.1, the strategy to train LW is the key to obtain working performance. Here, we propose a progressive training strategy. Experiments in Sec.4.3 show that without it, watermark injection and image quality maintenance cannot be reached at the same time. As shown in Fig.2 (b), the training strategy includes three steps, i.e. pre-training the message encoder and decoder, pre-training the message coupler and training the model formally. For the purpose of efficiency,  $z$  from training images encoded by  $Enc(\cdot)$ , rather than  $\tilde{z}$  from  $\epsilon_\theta(\tilde{z}_t, t)$ , is used in the training stage.

**Step 1: Pre-train the message encoder and decoder.** In this step, the encoded messages are input into the message decoder directly to train them in the self-supervision paradigm. The loss function in this step is  $\mathcal{L}_1$  in Eq.5:

$$\mathcal{L}_1 = \frac{1}{B \cdot n} \sum_{i=0}^{B-1} \sum_{k=0}^{n-1} (M_i^k - M_i^{k'})^2 \quad (5)$$

where  $M_i \in \{0, 1\}^n$  is the  $i$ -th randomly generated message,  $M_i^k$  is  $k$ -th bit of  $M_i$  and  $B$  is the batch size. When the exponential moving average of Bit Accuracy is higher than the threshold  $\tau_1$ , the step ends.

**Step 2: Pre-train the message coupler.** LW is expected to inject watermarks with minimizing any impact on image quality. Therefore, optimizing the parameters of the modules should be started from the initial state, i.e., outputting the same images as the vanilla model regardless of encoded messages. In this step, the coupler will be pre-trained as an

identity mapping of latent images. The loss function  $\mathcal{L}_2$  can be expressed as Eq.6:

$$\mathcal{L}_2 = \frac{1}{|\mathcal{D}|} \frac{1}{WH} \sum_{i \in \mathcal{D}} \|z_{i(0)} - z'_{i(0)}\|_2^2 \quad (6)$$

where  $\mathcal{D}$  is the training batch with the batch size  $|\mathcal{D}|$ ,  $W$  and  $H$  are the width and height of  $z_i$ , and  $z'_i$  is obtained using the same method outlined in Eq.3. When  $\mathcal{L}_2$  is lower than the threshold  $\tau_2$ , the step ends.

**Step 3: Train the model formally.** In this step, three loss functions, i.e.  $\mathcal{L}_z$ ,  $\mathcal{L}_I$  and  $\mathcal{L}_M$ , are used to train all the watermark-related modules. As shown in Eq.7,  $\mathcal{L}_z$  has the same form as Eq.6 and measures the L2 distance of latent images before and after message coupling:

$$\mathcal{L}_z = \frac{1}{|\mathcal{D}|} \frac{1}{WH} \sum_{i \in \mathcal{D}} \|z_{i(0)} - z'_{i(0)}\|_2^2. \quad (7)$$

And  $\mathcal{L}_I$  measures the visual similarity between images before and after injecting watermarks as shown in Eq.8:

$$\mathcal{L}_I = \frac{1}{|\mathcal{D}|} \sum_{i \in \mathcal{D}} LPIPS(x_i, Dec(z'_i)) \quad (8)$$

where  $LPIPS(\cdot, \cdot)$  is a commonly used method for visual similarity evaluation Zhang et al. [2018]. Inspired by Nguyen et al. [2023], we supervise the message encoding and decoding by Eq.9:

$$\mathcal{L}_M = \begin{cases} \frac{1}{|\mathcal{D}| \cdot n} \sum_{i \in \mathcal{D}} \sum_{k=0}^{n-1} (M_i^k - M_i^{k'})^2 & \text{if } BitACC < \tau_3 \\ \frac{1}{|\mathcal{D}|} \sum_{i \in \mathcal{D}} \log \left( \sum_{k=0}^{n-1} \exp (M_i^k - M_i^{k'})^2 \right) & \text{otherwise} \end{cases} \quad (9)$$

where  $BitACC$  represents Bit Accuracy and  $\tau_3$  is a threshold. When Bit Accuracy is high, the regression loss for bits is small and Eq.9 can help enhance the magnitude of the supervision signal. Finally, the loss function of Step 3 can be expressed by Eq.10:

$$\mathcal{L}_3 = \alpha_1 \mathcal{L}_z + \alpha_2 \mathcal{L}_I + \alpha_3 \mathcal{L}_M \quad (10)$$

where  $\alpha_1$ ,  $\alpha_2$  and  $\alpha_3$  are the weighting coefficients. The latent diffusion model is frozen throughout the three steps.

## 4 Experiments, Results and Discussions

### 4.1 Experiment Setup

#### 4.1.1 Datasets

Three datasets are used to train and evaluate LW. For training LW, 50,000 images are used. They are all randomly sampled from LAION-Aesthetics-5+ Schuhmann et al. [2022], which has 600M image-text pairs with predicted aesthetics scores of 5 or higher and is the training set for Stable Diffusion Rombach et al. [2022]. For evaluating LW and other methods, we randomly sample 5,000 captions from two datasets respectively, i.e. MS-COCO 2017 Lin et al. [2014] and Flickr30k Young et al. [2014], to generate images. And the captions from MS-COCO 2017 are all sampled in the val set.

#### 4.1.2 Watermark Baselines

Four recently proposed watermarking methods are used as our baselines for comparison, i.e. StegaStamp Tancik et al. [2020], StableSignature Fernandez et al. [2023], RoSteALS Bui et al. [2023] and TreeRing Wen et al. [2023]. For StegaStamp, RosteALS and StableSignature, the official codes and checkpoints are used to report the results on two evaluation datasets. The numbers of message bits for the three methods are 56, 56 and 48 respectively. For TreeRing, we follow the settings suggested by the paper using the official codes and inject random messages with a ring radius of 10.

### 4.1.3 LW Training

AdamW Loshchilov and Hutter [2018] is used to optimize the model. For the message encoder and decoder, the learning rate in Step 1 is set to  $1e-4$  and in Step 3 is  $1e-5$ . For the message coupler and decoupler, the learning rate in Step 2 is set to  $1e-3$  and in Step 3 is  $1e-5$ .  $\tau_1$ ,  $\tau_2$  and  $\tau_3$  are set to 0.990, 0.045 and 0.900.  $\alpha_1$ ,  $\alpha_2$  and  $\alpha_3$  are set to 1.5, 1.0 and 1.0 respectively. The batch size is 2. In Step 3, after the exponential moving average of Bit accuracy reaches 99.00%, we proceed to train the model for one more epoch and then terminate the training process. No data augmentation or noise layer is used during training. The latent diffusion model used in the experiments is Stable Diffusion v1.4. DDIM sampler Song et al. [2020] is used in the generation process and the sampling step is 50.

### 4.1.4 Attack Methods

The following 10 attacks are used for robustness evaluation in our experiments. It includes 9 single-attack scenarios and one all-attack scenario.

- Destructive attacks (single-attack scenario): Brightness distortion, contrast distortion, JPEG compression and Gaussian noising.
- Constructive attacks (single-attack scenario): Gaussian denoising and BM3D denoising Dabov et al. [2007].
- Reconstructive attacks (single-attack scenario) Zhao et al. [2023b]: SD (v2.1) Rombach et al. [2022], VAE-Cheng Cheng et al. [2020] and VAE-BMSHJ Ballé et al. [2018].
- All-attack (all-attack scenario): Use all the above attacks simultaneously.

### 4.1.5 Evaluation Metrics

Six metrics are used to evaluate image quality and watermark robustness. For image quality, two reference-based metrics, i.e. Frechet Inception Distance (FID) and Structural Similarity Index Measure (SSIM), and two no-reference metrics, i.e. Natural Image Quality Evaluator score (NIQE) Mittal et al. [2013] and Perception based Image Quality Evaluator score (PIQE) Venkatanath et al. [2015], are used. FID measures the distribution difference between watermarked and vanilla images. SSIM measures the similarity between them. NIQE and PIQE measure perceptual quality of images based on the statistical properties of natural images and human vision systems respectively. Vanilla images refer to the generated images by the same prompts with the same diffusion model but without using watermarking methods. Image quality is evaluated on untouched watermarked images, which suffer no attack. For watermark robustness, True Positive Rate at 0.01 False Positive Rate (TPR@0.01FPR) is used to quantify the performance of the identification task and Bit Accuracy is used to quantify the performance of the attribution task. We follow Fernandez et al. [2023], Zhao et al. [2023b] to calculate TPR@0.01FPR for all methods except TreeRing. For TreeRing, we follow the official paper and codes to report its TPR@0.01FPR.

## 4.2 Main Results

In Tab.1, we report an overview of image quality and watermark robustness results. From the perspective of image quality, among the previous methods, StableSignature achieves the best performance on three of the four metrics for COCO captions and two for Flickr. It demonstrates its superiority in terms of distribution consistency with vanilla images and visual quality compared to previous methods. StegaStamp performs second best on the whole for both evaluation sets. For RoSteALS, its poor PIQE on two evaluation sets shows its poor imperceptibility of watermarks. For TreeRing, its FID and SSIM are significantly inferior to others. It demonstrates that the images watermarked by TreeRing are significantly different from vanilla ones. Under the same number of message bits, LW exceeds or is equal to StegaStamp, RoSteALS and TreeRing on all four metrics (especially on FID, NIQE and PIQE), and exceeds StableSignature on three metrics. It shows that compared with the previous methods, LW can watermark generated images with the smallest difference and the closest perceptual quality to vanilla ones. When the number of message bits is 64 or even 128, LW is still superior in image quality.

From the perspective of watermark robustness, it can be seen that StegaStamp and RoSteALS have stronger resistance to the attacks than StableSignature and TreeRing. And the robustness of StegaStamp is stronger than RoSteALS, especially for the reconstructive attacks. When we focus on our proposed LW, under the same (48, 56) or even more number (64) of message bits, the average results on three attack categories are all higher than StegaStamp, about 3% higher on Bit Accuracy and about 5% higher on TPR. If we apply all attacks, the performance is still higher than StegaStamp. In particular, our TPR is as high as 99.52% on COCO captions and 99.74% on Flickr captions for 64 bits while it is difficult for other methods to achieve it. The results on the single-attack scenarios for COCO are shown in Tab.2 and for Flickr can be found in the supplementary material. Tab.2 shows that TPR of LW under each attack is near 100%

Table 1: The overview results on image quality and watermark robustness for previous methods (TreeRing Wen et al. [2023], Stable Signature (S.Signa.) Fernandez et al. [2023], RoSteALS Bui et al. [2023] and StegaStamp (S.Stamp) Tancik et al. [2020] ) and ours. D. Avg.: the average results on destructive attacks. C. Avg.: the average results on constructive attacks. R. Avg.: the average results on reconstructive attacks. Single Avg.: the average results on all single-attack scenarios. All: the results on the all-attack scenario. B.: Bit Accuracy (%). T.: TPR@0.01FPR (%). The numbers in parentheses are the numbers of encoded bits. **Mark** indicates B. and T. above 98.00%. **Bold** indicates image quality metrics that are better than or equal to the best previous methods.

Method	Untouched watermarked images						D. Avg.		C. Avg.		R. Avg.		Single Avg.		All	
	FID↓	SSIM↑	NIQE↓	PIQE↓	B.	T.	B.	T.	B.	T.	B.	T.	B.	T.	B.	T.
MS-COCO 2017 Evaluation Lin et al. [2014]																
TreeRing	12.95	0.02	13.05	11.95	-	97.40	-	82.35	-	59.90	-	38.93	-	62.89	-	5.20
S.Signa. (48)	<u>1.86</u>	0.92	<u>12.77</u>	<u>10.98</u>	99.45	100.0	94.08	<b>99.28</b>	84.60	91.84	59.83	34.82	80.56	76.14	46.44	0.02
RoSteALS (56)	7.33	0.93	15.81	44.35	96.69	94.69	96.38	94.50	96.61	94.73	85.10	74.07	92.67	87.74	82.51	94.47
S.Stamp (56)	7.39	<u>0.95</u>	16.91	11.33	96.98	94.69	96.85	94.70	96.92	94.68	94.27	94.90	96.00	94.76	88.03	94.11
Ours (48)	3.69	<b>0.97</b>	<b>12.12</b>	<b>10.11</b>	99.93	100.0	99.34	100.0	99.53	100.0	98.10	99.99	98.97	100.0	90.00	99.06
Ours (56)	3.96	<b>0.95</b>	<b>12.33</b>	<b>9.86</b>	99.89	100.0	99.40	100.0	99.49	99.76	98.20	100.0	99.02	99.95	89.79	99.52
Ours (64)	4.86	<b>0.95</b>	<b>12.33</b>	<b>10.01</b>	99.95	100.0	99.40	100.0	99.59	100.0	98.19	99.99	99.04	100.0	90.00	100.0
Ours (128)	3.26	<b>0.96</b>	<b>12.16</b>	<b>10.14</b>	99.45	100.0	96.10	99.97	98.04	100.0	93.66	99.96	95.72	99.97	83.56	99.72
Flickr30k Evaluation Young et al. [2014]																
TreeRing	14.59	0.02	13.48	<u>10.42</u>	-	89.10	-	78.65	-	58.65	-	42.73	-	62.23	-	7.50
S.Signa. (48)	<u>2.41</u>	0.93	<u>13.15</u>	10.52	99.69	100.0	94.84	<b>99.70</b>	86.24	96.20	59.99	36.51	81.31	77.86	46.99	0.04
RoSteALS (56)	9.91	0.93	16.31	44.98	96.49	94.60	96.26	94.67	96.46	94.67	93.37	94.68	95.34	94.67	83.27	94.80
S.Stamp (56)	7.37	<u>0.95</u>	17.49	11.01	96.96	94.66	96.85	94.73	96.97	94.69	94.21	94.63	96.00	94.69	88.25	94.24
Ours (48)	4.36	<b>0.97</b>	<b>12.43</b>	<b>9.57</b>	99.96	100.0	99.55	100.0	99.71	100.0	98.73	99.98	99.31	99.99	91.95	99.56
Ours (56)	5.81	<b>0.96</b>	<b>12.66</b>	<b>9.19</b>	99.52	100.0	99.02	100.0	99.48	100.0	98.85	100.0	99.06	100.0	91.96	99.92
Ours (64)	5.95	<b>0.95</b>	<b>12.64</b>	<b>9.40</b>	99.97	100.0	99.58	100.0	99.73	100.0	98.74	99.99	99.33	100.0	91.81	99.74
Ours (128)	3.88	<b>0.97</b>	<b>12.44</b>	<b>9.52</b>	99.84	100.0	96.76	100.0	98.75	100.0	94.94	100.0	95.60	100.0	85.24	99.82

Table 2: The results on the single-attack scenarios on MS-COCO 2017 captions. **Mark** indicates Bit Accuracy and TPR@0.01FPR above 98.00%.

Method	D. Attack				C. Attack		R. Attack		
	Bright	Contrast	JPEG	Noising	Gaussian	BM3D	SD (v2.1)	VAE (Cheng)	VAE (BMSHJ)
Bit Accuracy									
TreeRing	-	-	-	-	-	-	-	-	-
S.Signa. (48)	97.66	97.39	87.17	94.09	89.62	79.58	46.73	70.96	61.81
RoSteALS (56)	96.60	96.60	96.10	96.20	96.60	96.62	68.80	92.20	94.30
S.Stamp (56)	96.70	96.90	96.90	96.90	96.90	96.94	89.20	96.80	96.80
Ours (48)	99.73	99.82	99.44	98.36	99.91	99.14	99.09	97.27	97.93
Ours (56)	99.84	99.86	99.68	98.20	99.90	99.08	99.26	97.33	98.01
Ours (64)	99.81	99.86	99.50	98.43	99.93	99.25	99.19	97.44	97.95
Ours (128)	99.82	99.10	97.11	88.36	99.23	96.85	95.13	92.77	93.08
TPR@0.01FPR									
TreeRing	95.90	95.50	72.10	65.90	82.70	37.10	52.00	31.40	33.40
S.Signa. (48)	99.78	99.74	98.62	98.99	98.86	84.81	0.38	69.73	34.35
RoSteALS (56)	94.50	94.60	94.40	94.50	94.60	94.85	41.20	88.70	92.30
S.Stamp (56)	94.70	94.70	94.70	94.70	94.70	94.65	95.00	95.00	94.70
Ours (48)	100.0	100.0	100.0	100.0	100.0	100.0	100.0	99.96	100.0
Ours (56)	100.0	100.0	100.0	100.0	100.0	99.52	100.0	100.0	100.0
Ours (64)	100.0	100.0	100.0	100.0	100.0	100.0	100.0	99.96	100.0
Ours (128)	100.0	100.0	100.0	99.88	100.0	100.0	100.0	99.90	99.98

whether we encode 48, 56, 64 or 128 bits. When we inject 48, 56 and 64 bits, Bit Accuracy of LW under each attack is higher than 98%, except for VAE-Cheng and VAE-BMSHJ where it is higher than 97%. If we inject 128 bits, Bit Accuracy under six attacks drops but is still higher than 88%.

Finally, we give two examples of images watermarked by StegaStamp, RoSteALS and ours in Fig.3. It can be seen that the images watermarked by StegaStamp have obvious shadows at the edges and bright areas, and the images watermarked by RoSteALS are blurry while our method does not have the problems. Please refer to the supplementary material for more examples. In summary, compared with the previous methods, LW has stronger robustness and higher image quality, as shown in Fig.1.

### 4.3 Ablation Studies

#### 4.3.1 Training Strategy

To verify the effectiveness of each step in the three-step progressive training strategy, we plot the training curves of Bit Accuracy,  $\mathcal{L}_z$  (Eq.7) and  $\mathcal{L}_I$  (Eq.8) using one or more of the training steps in Fig.4. From Fig.4 (a), we can see that the message encoder and decoder cannot be optimized without Step 1. Fig.4 (b) and (c) show that LW converges faster and the difference between watermarked and vanilla images is smaller with Step 2. The training strategy can help LW have watermark injection and detection abilities while maintaining image quality better.

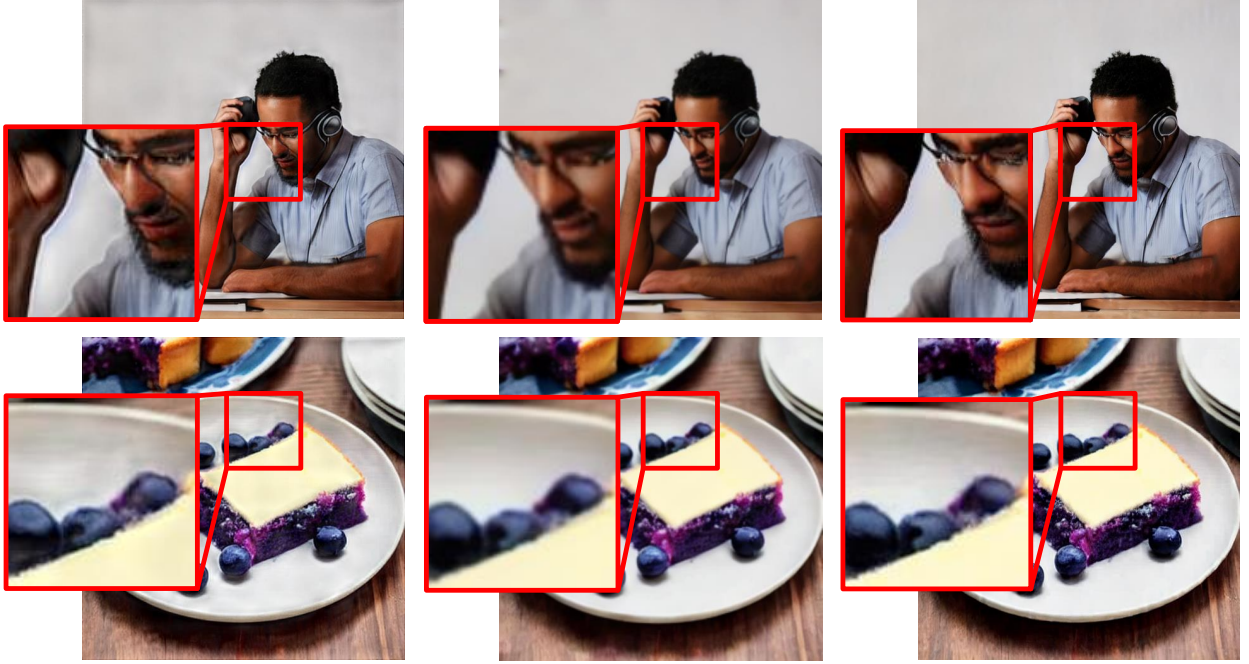


Figure 3: The images watermarked by StegaStamp Tancik et al. [2020] (left, 56 bits), RoSteALS Bui et al. [2023] (middle, 56 bits) and LW (right, 56 bits).

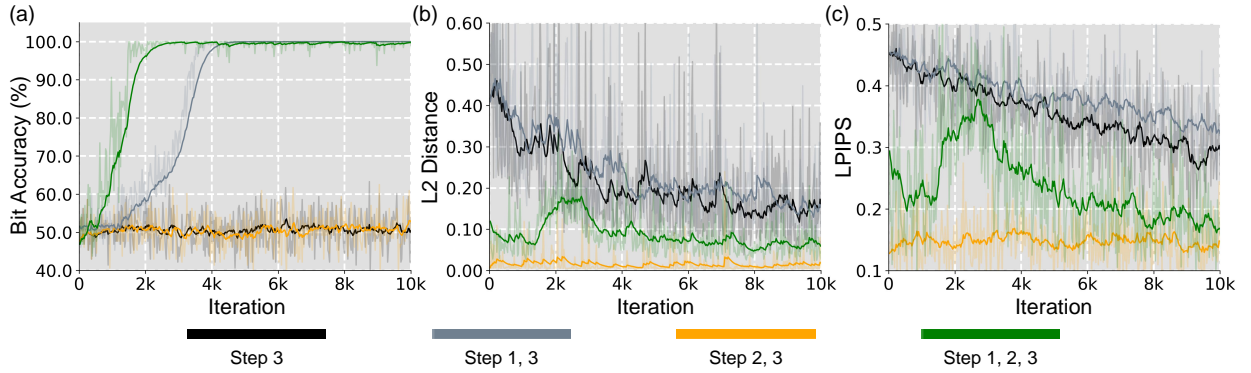


Figure 4: The training curves using one or more of the three steps of the progressive training strategy. (a) Bit Accuracy. (b) L2 distance of latent images (Eq.7). (c) Learned Perceptual Image Patch Similarity (LPIPS) loss Zhang et al. [2018] (Eq.8). Step 1 pre-trains the message encoder and decoder. Step 2 pre-trains the message coupler. Step 3 is the formal training.

### 4.3.2 Injection Channel

In Eq.3, encoded messages are coupled with Channel 0 of latent images. As reported in Tab.3, selecting other channel or all channels for watermark injection reduces robustness in most cases but sometimes it can improve image quality. Taking all the metrics into consideration, we select Channel 0 in the experiments.

## 4.4 Additional Discussions

### 4.4.1 Training Size

Fig.5 presents the results of watermark robustness and image quality by using 1, 10, 100, 1k, 10k and 50k images to train LW. It shows that various metrics tend to be stable when the size of training data is larger than 1k. In order to obtain better image quality, LW is trained on 50k images in the main experiments. The size of training data we use is

Table 3: The results of using different latent channel(s) for watermark injection on MS-COCO 2017 captions. The differences between using Channel 0 and other channel(s) are given. **Mark** denotes the decreasing metrics.

Channel(s)	Untouched watermarked images					D. Avg.	C. Avg.	R. Avg.	All Avg.	All
	FID↓	SSIM↑	NIQE↓	PIQE↓	B.	B.	B.	B.	B.	B.
0 (Used)	4.86	0.95	12.33	10.01	99.95	99.40	99.59	98.19	99.04	90.00
1	+1.05	+0.01	-0.21	-0.32	-0.46	-0.51	-0.98	-1.55	-0.96	+0.93
2	+2.09	-0.07	+0.20	-0.66	-0.10	-0.37	-1.39	-2.63	-1.35	-5.63
3	-2.07	-0.03	-0.21	-0.14	-0.04	-0.22	-0.35	-1.33	-0.62	-3.63
0,1,2,3	-3.65	+0.01	-0.71	+0.58	-0.16	-0.27	-0.86	-2.00	-0.98	-3.15

Table 4: The estimates of  $CO_2eq$  emission for Stable Diffusion v1.4 (SD v1.4) and LW. The data for SD v1.4 is from <https://huggingface.co/CompVis/stable-diffusion-v1-4>.

Method	Emission (kg)
SD v1.4	11,250
LW (48 bits)	1.27
LW (56 bits)	1.05
LW (64 bits)	1.12
LW (128 bits)	1.14

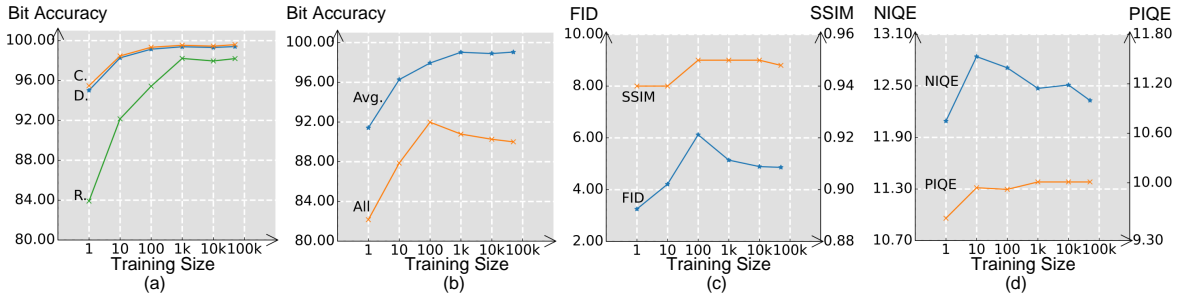


Figure 5: The change of performance with respect to the size of training data. (a) Average Bit Accuracy under the constructive (C.), destructive (D.) and reconstructive (R.) attacks. (b) Average Bit Accuracy under the single-attack scenarios (Avg.) and Bit Accuracy under the all-attack scenario (All). (c) FID (↓) and SSIM (↑). (d) NIQE (↓) and PIQE (↓).

lower than RoSteALS (100k) Bui et al. [2023]. StegaStamp Tancik et al. [2020] and StableSignature Fernandez et al. [2023] do not elaborate on how much training data from MIRFLICKR Huiskes and Lew [2008] and MS-COCO Lin et al. [2014] they use respectively.

#### 4.4.2 Environmental Impact

We estimate  $CO_2eq$  emission for training LW using Lacoste et al. [2019] in Tab.4. We do not consider memory storage, CPU-hours, production cost of GPUs / CPUs, etc. It shows that the emission by our training process is significantly lower than the vanilla generative model. LW is environmentally friendly and does not result in significant additional  $CO_2$  emission.

#### 4.4.3 Future Work

In the future, we will extend our method to other generative frameworks such as Generative Adversarial Networks, to explore the feasibility of rooting watermarks in the latent spaces of various generative models.

## 5 Conclusion

In this paper, we propose LW to root watermarks in latent space for latent diffusion models to identify and attribute generated images. Compared with previous methods, the fundamental difference is that the detection of watermarks is performed in latent space. This improvement, along with the proposed progressive training strategy, brings stronger robustness and higher image quality on two evaluation datasets at the same time. We provide an effective tool for distinguishing synthetic contents in the AIGC era.

## References

- Jonathan Ho, Ajay Jain, and Pieter Abbeel. Denoising diffusion probabilistic models. In *Proceedings of the Advances in Neural Information Processing Systems (NeurIPS)*, volume 33, pages 6840–6851, 2020.
- Jiaming Song, Chenlin Meng, and Stefano Ermon. Denoising diffusion implicit models. In *Proceedings of the International Conference on Learning Representations (ICLR)*, 2020.
- Alexander Quinn Nichol and Prafulla Dhariwal. Improved denoising diffusion probabilistic models. In *Proceedings of the International Conference on Machine Learning (ICML)*, pages 8162–8171, 2021.
- Luping Liu, Yi Ren, Zhijie Lin, and Zhou Zhao. Pseudo numerical methods for diffusion models on manifolds. In *Proceedings of the International Conference on Learning Representations (ICLR)*, 2022.
- Prafulla Dhariwal and Alexander Nichol. Diffusion models beat GANs on image synthesis. In *Proceedings of the Advances in Neural Information Processing Systems (NeurIPS)*, volume 34, pages 8780–8794, 2021.
- Alexander Quinn Nichol, Prafulla Dhariwal, Aditya Ramesh, Pranav Shyam, Pamela Mishkin, Bob McGrew, Ilya Sutskever, and Mark Chen. GLIDE: Towards photorealistic image generation and editing with text-guided diffusion models. In *Proceedings of the International Conference on Machine Learning (ICML)*, pages 16784–16804, 2022.
- Shuyang Gu, Dong Chen, Jianmin Bao, Fang Wen, Bo Zhang, Dongdong Chen, Lu Yuan, and Baining Guo. Vector quantized diffusion model for text-to-image synthesis. In *Proceedings of the IEEE/CVF Conference on Computer Vision and Pattern Recognition (CVPR)*, pages 10696–10706, 2022.
- Robin Rombach, Andreas Blattmann, Dominik Lorenz, Patrick Esser, and Björn Ommer. High-resolution image synthesis with latent diffusion models. In *Proceedings of the IEEE/CVF Conference on Computer Vision and Pattern Recognition (CVPR)*, pages 10684–10695, 2022.
- Edward J Hu, Phillip Wallis, Zeyuan Allen-Zhu, Yanzhi Li, Shean Wang, Lu Wang, Weizhu Chen, et al. LoRA: Low-rank adaptation of large language models. In *Proceedings of the International Conference on Learning Representations (ICLR)*, 2021.
- Nataniel Ruiz, Yuanzhen Li, Varun Jampani, Yael Pritch, Michael Rubinstein, and Kfir Aberman. DreamBooth: Fine tuning text-to-image diffusion models for subject-driven generation. In *Proceedings of the IEEE/CVF Conference on Computer Vision and Pattern Recognition (CVPR)*, pages 22500–22510, 2023.
- Enze Xie, Lewei Yao, Han Shi, Zhili Liu, Daquan Zhou, Zhaoqiang Liu, Jiawei Li, and Zhenguo Li. DiffFit: Unlocking transferability of large diffusion models via simple parameter-efficient fine-tuning. In *Proceedings of the IEEE/CVF International Conference on Computer Vision (ICCV)*, pages 4230–4239, 2023.
- Midjourney. <https://www.midjourney.com/home/>, 2022.
- Wukong. <https://xihe.mindspore.cn/modelzoo/wukong>, 2022.
- HuggingFace. <https://huggingface.co/>.
- Clark Barrett, Brad Boyd, Elie Bursztein, Nicholas Carlini, Brad Chen, Jihye Choi, Amrita Roy Chowdhury, Mihai Christodorescu, Anupam Datta, Soheil Feizi, et al. Identifying and mitigating the security risks of generative AI. *Foundations and Trends in Privacy and Security (FTPS)*, 6(1):1–52, 2023.
- Sheng-Yu Wang, Oliver Wang, Richard Zhang, Andrew Owens, and Alexei A Efros. CNN-generated images are surprisingly easy to spot... for now. In *Proceedings of the IEEE/CVF Conference on Computer Vision and Pattern Recognition (CVPR)*, pages 8695–8704, 2020.
- Yuyang Qian, Guojun Yin, Lu Sheng, Zixuan Chen, and Jing Shao. Thinking in frequency: Face forgery detection by mining frequency-aware clues. In *Proceedings of the European Conference on Computer Vision (ECCV)*, pages 86–103, 2020.
- Ke Sun, Hong Liu, Taiping Yao, Xiaoshuai Sun, Shen Chen, Shouhong Ding, and Rongrong Ji. An information theoretic approach for attention-driven face forgery detection. In *Proceedings of the European Conference on Computer Vision (ECCV)*, pages 111–127, 2022.
- Zhendong Wang, Jianmin Bao, Wengang Zhou, Weilun Wang, Hezhen Hu, Hong Chen, and Houqiang Li. DIRE for diffusion-generated image detection. In *Proceedings of the IEEE/CVF International Conference on Computer Vision (ICCV)*, pages 22445–22455, 2023a.
- Lucy Chai, David Bau, Ser-Nam Lim, and Phillip Isola. What makes fake images detectable? Understanding properties that generalize. In *Proceedings of the European Conference on Computer Vision (ECCV)*, pages 103–120, 2020.
- Riccardo Corvi, Davide Cozzolino, Giada Zingarini, Giovanni Poggi, Koki Nagano, and Luisa Verdoliva. On the detection of synthetic images generated by diffusion models. In *Proceedings of the IEEE International Conference on Acoustics, Speech and Signal Processing (ICASSP)*, pages 1–5, 2023.

- Peter Lorenz, Ricard L. Durall, and Janis Keuper. Detecting images generated by deep diffusion models using their local intrinsic dimensionality. In *Proceedings of the IEEE/CVF International Conference on Computer Vision Workshops (ICCVW)*, pages 448–459, 2023.
- Jonas Ricker, Simon Damm, Thorsten Holz, and Asja Fischer. Towards the detection of diffusion model deepfakes. In *Proceedings of the International Conference on Learning Representations (ICLR)*, 2023.
- Ashif Raja. Active and passive detection of image forgery: A review analysis. *International Journal of Engineering Research and Technology (IJERT)*, 9(5):418–424, 2021.
- Xiaoshuai Wu, Xin Liao, and Bo Ou. SepMark: Deep separable watermarking for unified source tracing and deepfake detection. In *Proceedings of the 31st ACM International Conference on Multimedia (MM)*, page 1190–1201, 2023.
- Pierre Fernandez, Alexandre Sablayrolles, Teddy Furon, Hervé Jégou, and Matthijs Douze. Watermarking images in self-supervised latent spaces. In *Proceedings of the IEEE International Conference on Acoustics, Speech and Signal Processing (ICASSP)*, pages 3054–3058, 2022.
- Matthew Tancik, Ben Mildenhall, and Ren Ng. Stegastamp: Invisible hyperlinks in physical photographs. In *Proceedings of the IEEE/CVF Conference on Computer Vision and Pattern Recognition (CVPR)*, pages 2117–2126, 2020.
- Cheng Xiong, Chuan Qin, Guorui Feng, and Xinpeng Zhang. Flexible and secure watermarking for latent diffusion model. In *Proceedings of the 31st ACM International Conference on Multimedia (MM)*, pages 1668–1676, 2023.
- Quang Nguyen, Truong Vu, Cuong Pham, Anh Tran, and Khoi Nguyen. Stable Messenger: Steganography for message-concealed image generation. *arXiv preprint arXiv:2312.01284*, 2023.
- Tu Bui, Shruti Agarwal, Ning Yu, and John Collomosse. RoSteALS: Robust steganography using autoencoder latent space. In *Proceedings of the IEEE/CVF Conference on Computer Vision and Pattern Recognition (CVPR)*, pages 933–942, 2023.
- Zhenting Wang, Chen Chen, Yuchen Liu, Lingjuan Lyu, Dimitris Metaxas, and Shiqing Ma. How to detect unauthorized data usages in text-to-image diffusion models. *arXiv preprint arXiv:2307.03108*, 2023b.
- Pierre Fernandez, Guillaume Couairon, Hervé Jégou, Matthijs Douze, and Teddy Furon. The stable signature: Rooting watermarks in latent diffusion models. In *Proceedings of the IEEE/CVF International Conference on Computer Vision (ICCV)*, pages 22466–22477, 2023.
- Yunqing Zhao, Tianyu Pang, Chao Du, Xiao Yang, Ngai-Man Cheung, and Min Lin. A recipe for watermarking diffusion models. *arXiv preprint arXiv:2303.10137*, 2023a.
- Yuxin Wen, John Kirchenbauer, Jonas Geiping, and Tom Goldstein. Tree-Ring watermarks: Fingerprints for diffusion images that are invisible and robust. In *Proceedings of the Advances in Neural Information Processing Systems (NeurIPS)*, 2023.
- Xuandong Zhao, Kexun Zhang, Yu-Xiang Wang, and Lei Li. Generative autoencoders as watermark attackers: Analyses of vulnerabilities and threats. In *Proceedings of the International Conference on Machine Learning Workshop (ICMLW)*, 2023b.
- Tsung-Yi Lin, Michael Maire, Serge Belongie, James Hays, Pietro Perona, Deva Ramanan, Piotr Dollár, and C Lawrence Zitnick. Microsoft COCO: Common objects in context. In *Proceedings of the European Conference on Computer Vision (ECCV)*, pages 740–755, 2014.
- Xin Wang, Yudong Chen, and Wenwu Zhu. A survey on curriculum learning. *IEEE Transactions on Pattern Analysis and Machine Intelligence (TPAMI)*, 44(9):4555–4576, 2021.
- Richard Zhang, Phillip Isola, Alexei A Efros, Eli Shechtman, and Oliver Wang. The unreasonable effectiveness of deep features as a perceptual metric. In *Proceedings of the IEEE Conference on Computer Vision and Pattern Recognition (CVPR)*, pages 586–595, 2018.
- Jari Korhonen and Junyong You. Peak signal-to-noise ratio revisited: Is simple beautiful? In *Proceedings of the Fourth International Workshop on Quality of Multimedia Experience (QoMEX)*, pages 37–38, 2012.
- Zhou Wang, Alan C Bovik, Hamid R Sheikh, and Eero P Simoncelli. Image quality assessment: From error visibility to structural similarity. *IEEE Transactions on Image Processing (TIP)*, 13(4):600–612, 2004.
- Christoph Schuhmann, Romain Beaumont, Richard Vencu, Cade Gordon, Ross Wightman, Mehdi Cherti, Theo Coombes, Aarush Katta, Clayton Mullis, Mitchell Wortsman, et al. Laion-5b: An open large-scale dataset for training next generation image-text models. In *Proceedings of the Advances in Neural Information Processing Systems (NeurIPS)*, volume 35, pages 25278–25294, 2022.
- Jia Deng, Wei Dong, Richard Socher, Li-Jia Li, Kai Li, and Li Fei-Fei. ImageNet: A large-scale hierarchical image database. In *Proceedings of the IEEE/CVF Conference on Computer Vision and Pattern Recognition (CVPR)*, pages 248–255, 2009.

- Olaf Ronneberger, Philipp Fischer, and Thomas Brox. U-net: Convolutional networks for biomedical image segmentation. In *Proceedings of the 18th Medical Image Computing and Computer-Assisted Intervention (MICCAI)*, pages 234–241, 2015.
- Ilya Loshchilov and Frank Hutter. Decoupled weight decay regularization. In *Proceedings of the International Conference on Learning Representations (ICLR)*, 2018.
- Ingemar J. Cox, Matthew J. Miller, Jeffrey A. Bloom, Jessica Fridrich, and Ton Kalker. Digital watermarking and steganography. *Morgan Kaufmann*, 2007.
- Kevin Alex Zhang, Lei Xu, Alfredo Cuesta-Infante, and Kalyan Veeramachaneni. Robust invisible video watermarking with attention. *arXiv preprint arXiv:1909.01285*, 2019.
- Johannes Ballé, David Minnen, Saurabh Singh, Sung Jin Hwang, and Nick Johnston. Variational image compression with a scale hyperprior. In *Proceedings of the International Conference on Learning Representations (ICLR)*, 2018.
- Zhengxue Cheng, Heming Sun, Masaru Takeuchi, and Jiro Katto. Learned image compression with discretized gaussian mixture likelihoods and attention modules. In *Proceedings of the IEEE/CVF Conference on Computer Vision and Pattern Recognition (CVPR)*, pages 7939–7948, 2020.
- Yixiong Chen. X-iqe: explainable image quality evaluation for text-to-image generation with visual large language models. *arXiv preprint arXiv:2305.10843*, 2023.
- Ning Yu, Vladislav Skripniuk, Sahar Abdelnabi, and Mario Fritz. Artificial fingerprinting for generative models: Rooting deepfake attribution in training data. In *Proceedings of the IEEE/CVF International Conference on Computer Vision (ICCV)*, pages 14448–14457, 2021.
- Alexandre Lacoste, Alexandra Luccioni, Victor Schmidt, and Thomas Dandres. Quantifying the carbon emissions of machine learning. In *Proceedings of the Advances in Neural Information Processing Systems Workshop (NeurIPSW)*, 2019.
- Anish Mittal, Rajiv Soundararajan, and Alan C. Bovik. Making a "completely blind" image quality analyzer. *IEEE Signal Processing Letters*, 20(3):209–212, 2013.
- Jascha Sohl-Dickstein, Eric Weiss, Niru Maheswaranathan, and Surya Ganguli. Deep unsupervised learning using nonequilibrium thermodynamics. In *Proceedings of the International Conference on Machine Learning (ICML)*, pages 2256–2265, 2015.
- Kostadin Dabov, Alessandro Foi, Vladimir Katkovnik, and Karen Egiazarian. Image denoising by sparse 3-d transform-domain collaborative filtering. *IEEE Transactions on Image Processing (TIP)*, 16(8):2080–2095, 2007.
- Peter Young, Alice Lai, Micah Hodosh, and Julia Hockenmaier. From image descriptions to visual denotations: New similarity metrics for semantic inference over event descriptions. *Transactions of the Association for Computational Linguistics (TACL)*, 2:67–78, 2014.
- N Venkatanath, D Praneeth, Maruthi Chandrasekhar Bh, Sumohana S Channappayya, and Swarup S Medasani. Blind image quality evaluation using perception based features. In *IEEE National Conference on Communications (NCC)*, pages 1–6, 2015.
- Mark J Huiskes and Michael S Lew. The mir flickr retrieval evaluation. In *Proceedings of the 1st ACM International Conference on Multimedia Information Retrieval (ICMIR)*, pages 39–43, 2008.

## Appendix A Detailed Results on Flickr30k

The results on Flickr30k captions under the single-attack scenarios are shown in Tab.S1.

Table S1: The results on Flickr30k captions under the single-attack scenarios. D. Attack: the destructive attacks. C. Attack: the constructive attacks. R. Attack: the reconstructive attacks. The numbers in parentheses are the numbers of encoded bits. **Mark** indicates Bit Accuracy and TPR@0.01FPR above 98.00%.

Method	D. Attack				C. Attack		R. Attack		
	Bright	Contrast	JPEG	Noising	Gaussian	BM3D	SD (v2.1)	VAE (Cheng)	VAE (BMSHJ)
Bit Accuracy									
TreeRing	-	-	-	-	-	-	-	-	-
S.Signa. (48)	98.19	97.95	87.88	95.33	90.43	82.05	45.72	71.44	62.80
RoSteALS (56)	96.49	96.43	96.03	96.09	96.50	96.41	90.32	94.77	95.03
S.Stamp (56)	96.84	96.75	96.96	96.86	96.98	96.95	88.91	96.83	96.89
Ours (48)	99.81	99.88	99.61	98.91	99.94	99.48	99.22	98.31	98.67
Ours (56)	99.17	99.20	99.18	98.51	99.44	99.51	99.14	98.74	98.68
Ours (64)	99.85	99.90	99.66	98.90	99.95	99.51	99.32	98.30	98.60
Ours (128)	99.56	99.56	97.89	90.03	99.62	97.87	95.76	94.46	94.61
TPR@0.01FPR									
TreeRing	87.80	87.70	74.80	64.30	78.00	39.30	56.50	34.50	37.20
S.Signa. (48)	99.94	99.88	99.43	99.56	99.40	92.99	0.12	71.98	37.44
RoSteALS (56)	94.66	94.66	94.64	94.72	94.64	94.69	94.54	94.78	94.72
S.Stamp (56)	94.76	94.76	94.70	94.68	94.70	94.68	94.40	94.72	94.78
Ours (48)	100.0	100.0	100.0	100.0	100.0	100.0	100.0	99.96	99.98
Ours (56)	100.0	100.0	100.0	100.0	100.0	100.0	100.0	100.0	100.0
Ours (64)	100.0	100.0	100.0	100.0	100.0	100.0	100.0	99.98	99.98
Ours (128)	100.0	100.0	100.0	99.98	100.0	100.0	100.0	100.0	100.0

## Appendix B Examples of LW-Watermarked Images

The examples of images watermarked by LW are shown in Fig.S1 (48 bits), Fig.S2 (56 bits), Fig.S3 (64 bits) and Fig.S4 (128 bits).

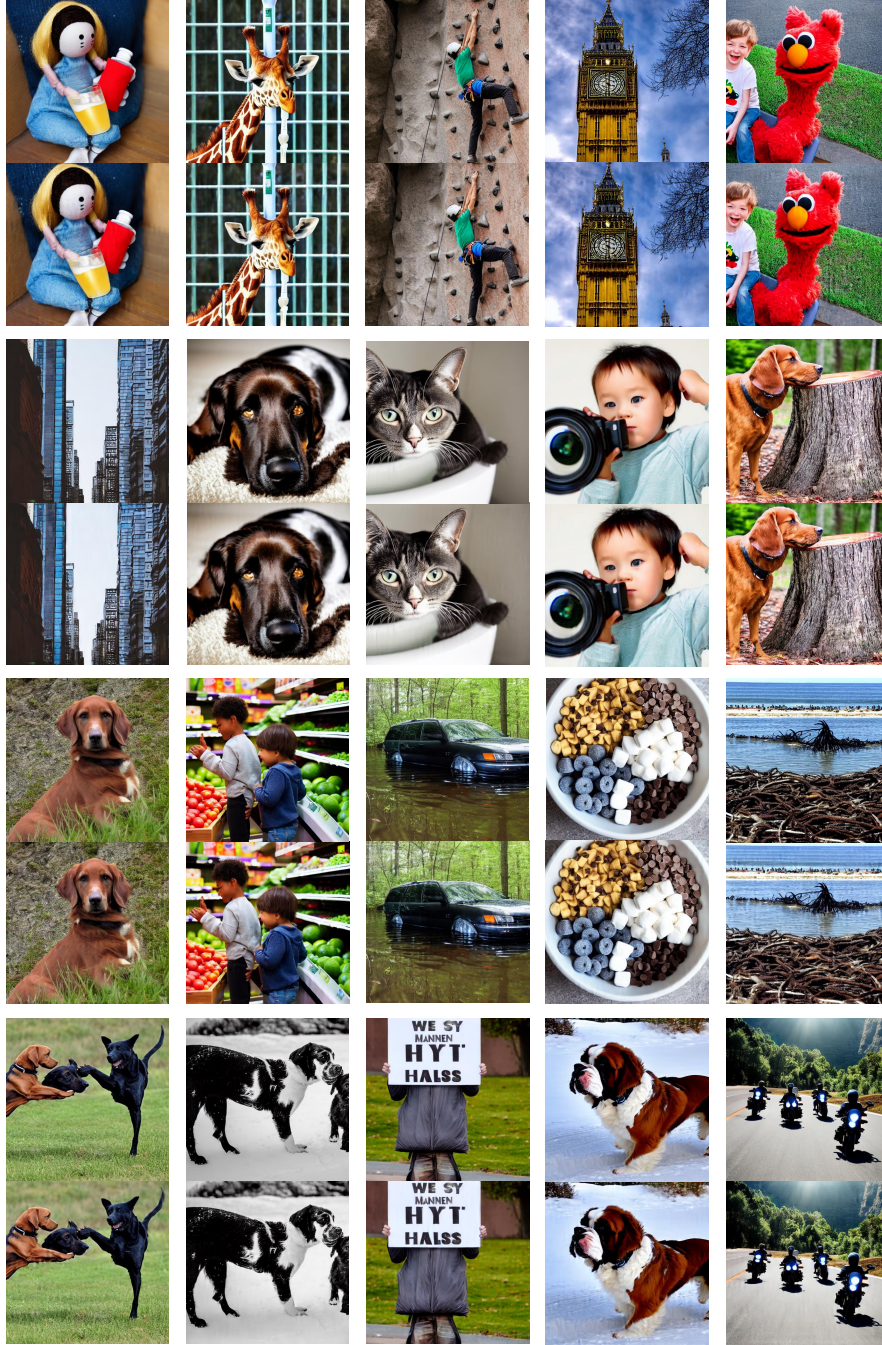


Figure S1: The examples of images watermarked by LW (48 bits). The top of each set is the vanilla image generated by Stable Diffusion, and the bottom is the image watermarked by LW.

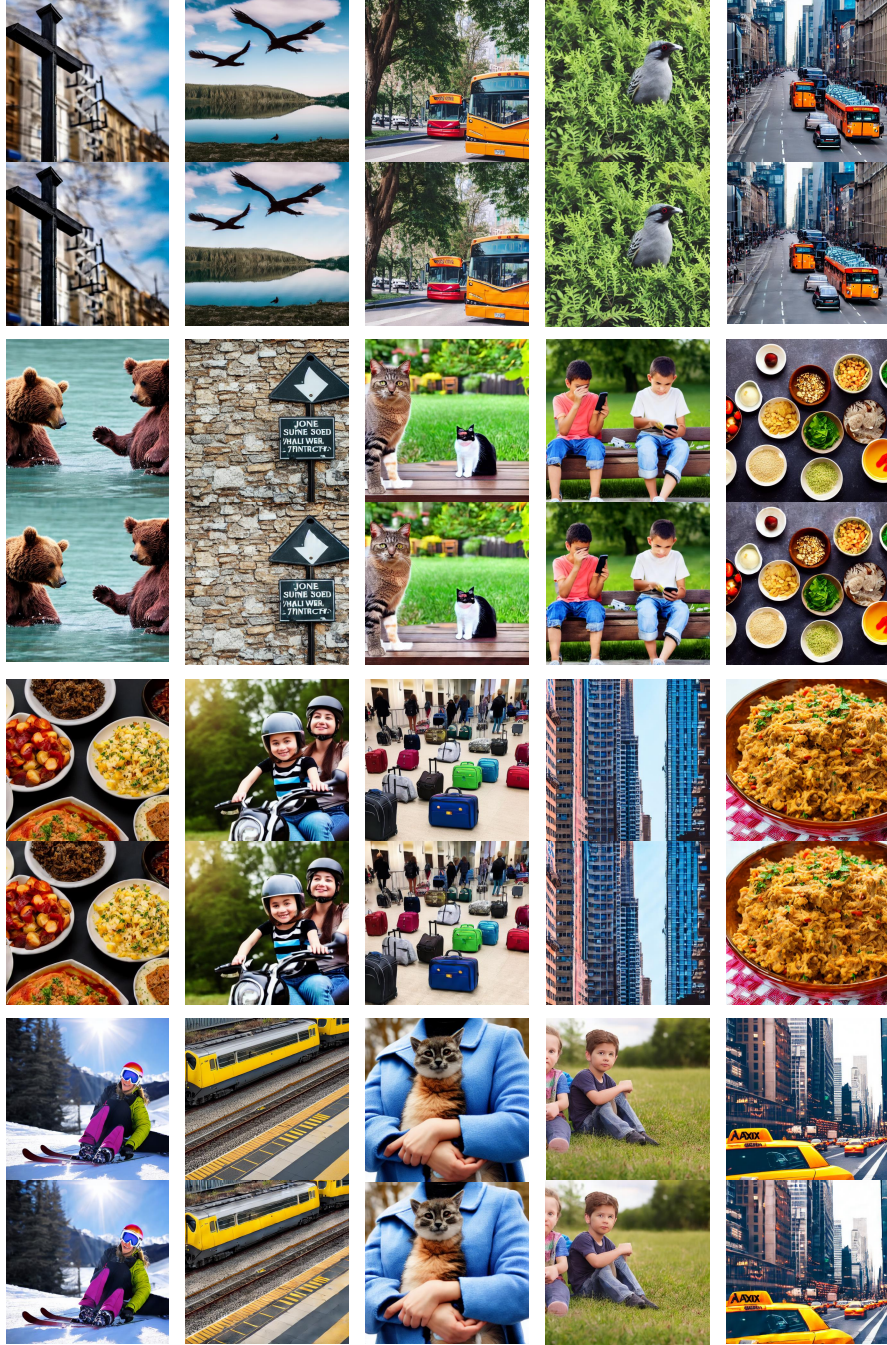


Figure S2: The examples of images watermarked by LW (56 bits). The top of each set is the vanilla image generated by Stable Diffusion, and the bottom is the image watermarked by LW.

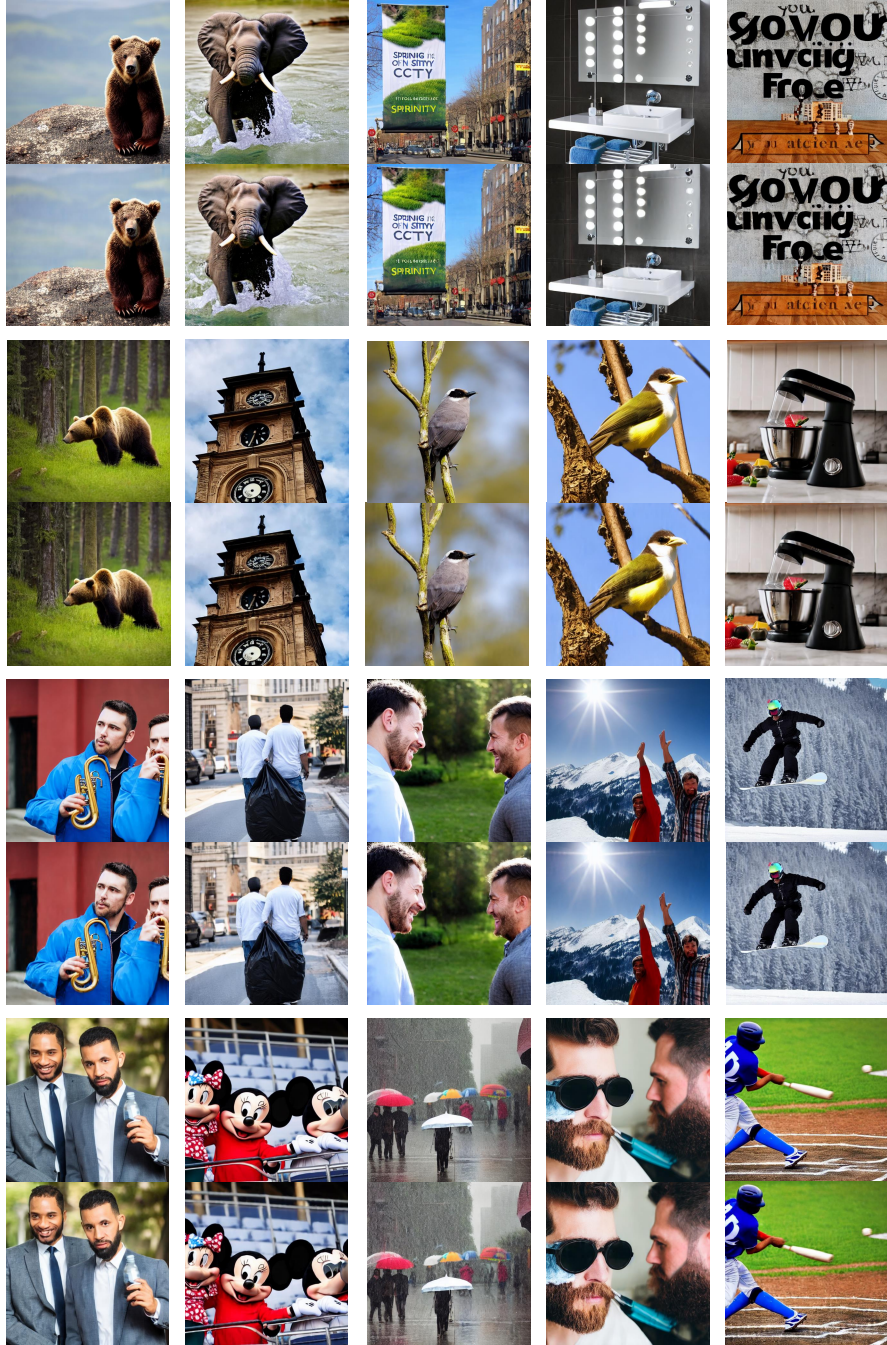


Figure S3: The examples of images watermarked by LW (64 bits). The top of each set is the vanilla image generated by Stable Diffusion, and the bottom is the image watermarked by LW.

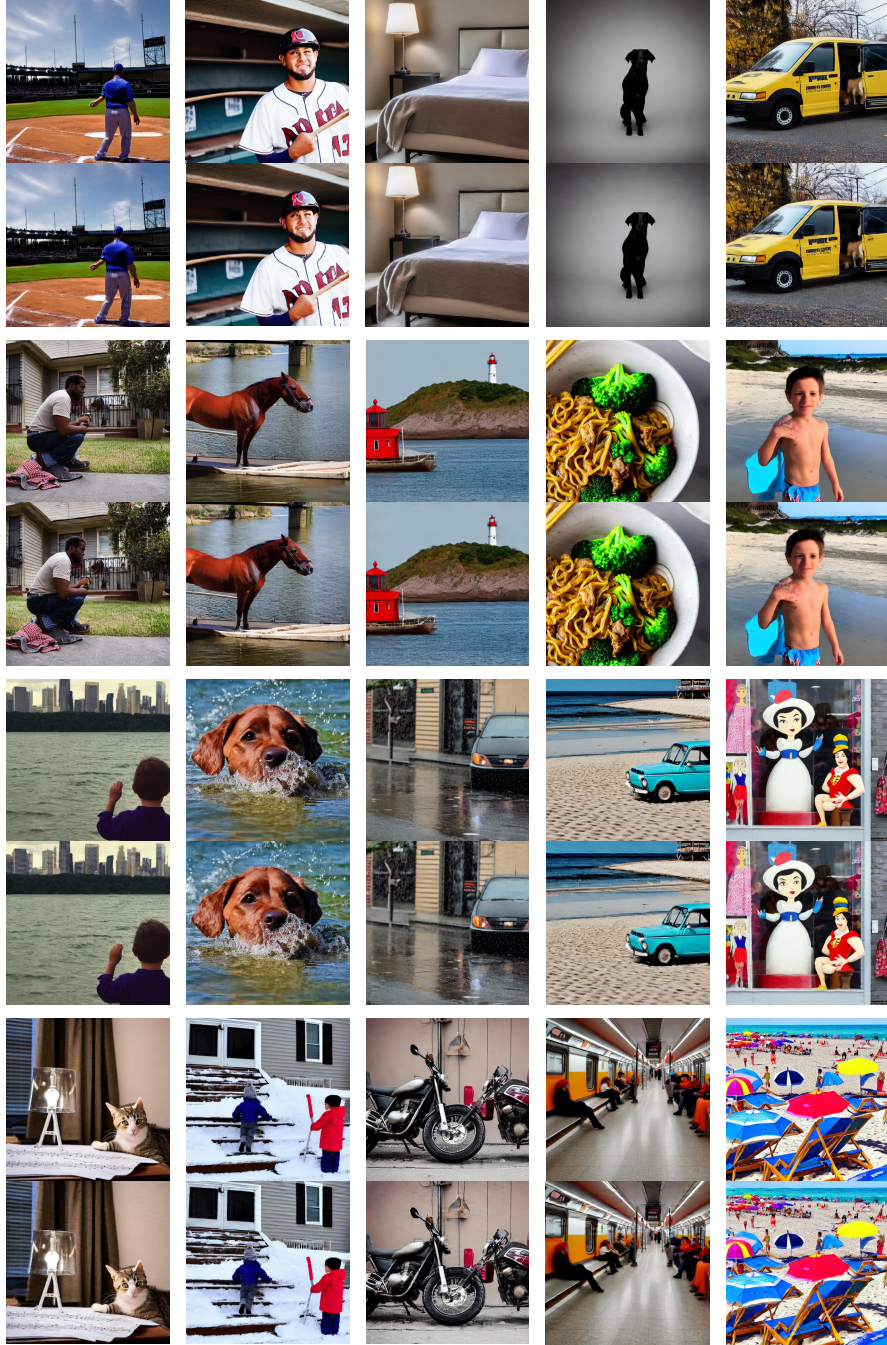


Figure S4: The examples of images watermarked by LW (128 bits). The top of each set is the vanilla image generated by Stable Diffusion, and the bottom is the image watermarked by LW.